Enhanced photoelectrochemical response of 1D TiO_2 by atmospheric pressure plasma surface modification

Vinayak Vitthal Satale[1, 2], Vattikondala Ganesh[2], Avishek Dey[3], Satheesh Krishnamurthy[3,*] and S. Venkataprasad Bhat[1, 2,*]

[1]SRM Research Institute, SRM Institute of Science and Technology, Kattankulathur-603203, Tamil Nadu, India
[2]Department of Physics & Nanotechnology, SRM Institute of Science and Technology, Kattankulathur-603203, Tamil Nadu, India
[3]School of Engineering and Innovation, The Open University, Milton Keynes, MK76 AA, United Kingdom

[*]Corresponding author: venkatab@srmist.edu.in; satheesh.krishnamurthy@open.ac.uk

Abstract:

In this paper we demonstrate the use of atmospheric pressure plasma jet (APPJ) to functionalize the surface of hydrothermally synthesized vertically aligned TiO_2 nanorods (TNRs) for photo electrochemical (PEC) application. The TNRs functionalized with the atmospheric pressure He-plasma showed relatively higher crystallinity, improved light absorption, and change in the morphology with additional surface area, leading to an enhanced photocurrent density than that of the untreated. Achieving the PEC performance on par with the best in the literature, this APPJ treatment is shown to be a promising technique to obtain better functionality with TNR kind of materials and many other nano-micro systems for various applications such as PEC hydrogen generation.

Keywords: One-dimensional, atmospheric-plasma-jet, functionalization, photoelectrochemical.

1. Introduction:

TiO_2 has been widely explored for thin film solar cells [1], photocatalytic H_2 evolution [2], photo-electrochemical (PEC) water splitting [3], self-cleaning and antifogging applications [4] due to its optical and electronic properties along with the nontoxicity, economical, chemical stability, and anticorrosive characteristics [5]. TiO_2 finds valuable applications in LEDs, as photo-anode in new photovoltaic devices, photoelectrochemical cells, water splitting, and in gas sensors & heat reflectors [6–12]. Of particular interest are, one-dimensional TiO_2 nanorod (TNR) arrays fabricated by a simple and economical hydrothermal method [13], found to have a superior chemical stability and high electron mobility [14,15] that are required for all the above applications. Furthermore, for solar energy applications, the vertical alignment of nanorods on a substrate can offer improved absorption of light due to the diffuse reflection happening between the nanorod arrays. Also, such structures offer a direct and efficient transport pathway for the photo-generated electrons. Altogether, these features are expected to enhance the carrier generation, their separation, and transport in solar energy conversion devices [16]. However, the wide band-gap of the TiO_2 (3.2 eV) limits its light-absorption only to the UV range, which is only a small part of the solar spectrum [17]. Hence, bandgap engineering of TiO_2 has been explored through metal, non-metal doping [18], and also metal doping with Ar, N_2, & O_2 plasma treatment [19] to improve the absorption of the solar radiation. Such efforts on improving the optical properties of TiO_2 film with & without doping have been made by employing the plasma treatment technique [20]. In another way, many methods for its surface modification have been practiced including surface hydrogenation, vacuum activation and plasma treatment [21–23]. The plasma treatment cover's a very broad range of different plasma techniques based on the operating pressure (low and atmospheric), thermodynamics (thermal and non-thermal), temperature (low and high), source of plasma (Microwave discharge, DC discharge, dielectric barrier discharge, corona discharge, AC arc discharge, electron beam, plasma torch, glow discharge, hollow cathode discharge) [24–36].

Among them, non-thermal and atmospheric pressure plasmas have grown to be of huge scientific and commercial importance for materials processing due to their simple cost effective nature and ability to bring in rich chemical as well as physical properties [37,38]. Plasma treatment technique has been the most versatile surface treatment [39–42] based on a few of its advantages namely; (i) the air plasma treatment removes organic impurities absorbed on the surface of TiO_2, (ii) formation of hydroxyl group on the surface during the plasma treatment to improve wettability [43], and (iii)

oxygen vacancies might serve as the trap centers for photo-generated electrons and suppress the recombination. Hence, the electron-hole pairs could be separated and transported more effectively [44]. For example, the plasma treatment of TNRs with reactive gases such as H_2, N_2, and O_2 has been explored and an improved the PCE efficiency from 0.62 % (untreated) to 1.11 % (N_2 plasma-treated) of DSSCs [45].

Several efforts were made to improve the PEC activity of TiO_2 nanostructures. TiO_2 nanoparticle layer synthesized on Ti foil via the potentiostatic anodization method showed a PEC current density of 2 μAcm^{-2} and further improved up to 40 μAcm^{-2} after combining it with Cu_2O [46]. The photocurrent density up to 1 $mAcm^{-2}$ was achieved with TiO_2 nanoporous photoelectrodes with mixed anatase and rutile phases by a dip-coating and subsequent calcination process [47]. Further, the PEC performance of TiO_2 was also improved by doping such as Fe, N, Mn, Cr, Si, Co [48–51]. Particularly, Fe doped TiO_2 nanoparticles exhibited a photocurrent density of 54 μAcm^{-2}, which was 3.6 times higher than that of un-doped TiO_2 nanoparticles [52]. Peng et al. reported the N-doped TiO_2 (P25 Degussa) for photoelectrochemical CO_2 reduction and achieved the maximum current density of 0.104 $mAcm^{-2}$ at 2 V (vs. SCE) [53]. N doping of anatase and rutile phase TiO_2 nanowires also improved the PEC performance [54,55]. The activity of TNRs was improved up to 1.25, 2.0, 1.53 $mAcm^{-2}$ (vs. Ag/AgCl) and 0.81 $mAcm^{-2}$ (vs. RHE), by doping of C, Sn, W and Si [56–59]. The hydrogenation of TNR via rapid thermal annealing (RTA) process was also explored for PEC H_2 evolution. The highest photocurrent of 3.7 $mAcm^{-2}$ was obtained using TNRs treated with RTA at 400 ^oC for 1 hr [60].

Few of such efforts to improve the PEC performance of TiO_2 were involving the conventional plasma. The TiO_2 nanotubes treated under vacuum with air plasma for 20 minutes also showed a stable & improved photocurrent density (2.4 $mAcm^{-2}$ vs. RHE) [43]. The TiO_2 thin film deposited by the atomic layer deposition method showed enhancement in the PEC current density from 0.12 to 1 $mAcm^{-2}$ after hydrogen plasma treatment [61]. TiO_2 nanosheets plasma-treated using a plasma cleaner under Ar atmosphere showed the current density of 43.7 μAcm^{-2}(vs. Ag/AgCl) under 300 W Xenon arc lamp with an AM 1.5 filter [62]. In another report, after incorporation of hydrogen by H_2 plasma treatment, the mesoporous TiO_2 films showed the current densities of 22.9 μAcm^{-2} & 0.16 μAcm^{-2} under UV-LED & Blue-LED respectively [63]. Thus, in general, the conventional plasma treatment was already proved to be an effective technique to improve the PEC performance of TiO_2. The plasma treatment is also known to improve the functional properties in many other

materials as well [64–66] and for example, it has also been reported that helium (He) plasma treatment is a promising method to reduce the contact resistance of source/drain region for Indium-Gallium-Zinc oxide (IGZO) thin film transistors [64] due to the formation of oxygen vacancies [65].

One-dimensional TNRs could offer an advantageous conducting network because of their short electron pathway as discussed in the works of literature [16]. Thus, it was expected that the nanorods would show a better PEC performance with higher photocurrent density. However, it can be also observed from the literature that they generally showed relatively inferior PEC activity with lower photocurrent, probably due to the lower crystallinity, higher contact angle with water, as well as due to the absence of surface defect states. Few efforts, as mentioned above, were made to overcome these limitations and to improve the PEC performance of TNRs. However, most of these efforts used the plasma treatment process under vacuum and high temperature conditions. As reported, the low-power atmospheric pressure plasma jet (APPJ) is an easily scalable, non-thermal technique to improve the electronic properties of many functional materials [67–69]. Presently, there has been an increasing interest for APPJ in materials processing, as there is no requirement for sophisticated vacuum equipment and high temperatures which makes it cost effective [38,69]. Additionally, plasma jets can be directed towards substrated, hence can be used remotely suitable for industrial applications. APPJ is known to control the defects, crystallinity, and surface wettability [68–70]. APPJs can deliver transient electric fields along with charged particles, neutral metastable species, radicals, and radiation in the UV and visible regions conveniently in a processing plume [68,71]. To overcome the small area covered by the plasma jet on the substrate, several approaches have been reported so far, e.g. array of plasma jet or by varying the plasmas jet operating conditions [72–75].

It can be expected that the functionalization of TNRs using APPJ could improve the optical, electrical, and interface properties between TNR and electrolyte resulting in better PEC performance. Being a simple technique, which consumes minimum time and can be done at room temperature, this could prove to be a quick and cool tool to use even with flexible substrates. Such functionalized TNRs with atmospheric pressure plasma treatment at room temperature are not reported to the best of our knowledge. Herein, we demonstrate for the first time, the room temperature APPJ surface modification of high performance 1D TNR arrays that are grown by a simple, one-step hydrothermal process on FTO substrate. We chose He, ($He+O_2$), & ($He+N_2$) as

carrier gases to modify the surface of the 1D TNR and observed the changes leading to enhanced photoelectrochemical activity.

2. Experimental:

2.1. Preparation of TiO_2 nanorods:

One dimensional TiO_2 nanorods (TNRs) were prepared via a simple hydrothermal route by following the procedure reported in the literature [76]. In a typical synthesis, the $TiCl_4$ was added to the mixture of concentrated hydrochloric acid (HCl) and DI water (1:1 solution) followed by stirring for 30 min. The solution was then transferred into a Teflon coated 50 ml autoclave with pre-cleaned Fluorine-doped tin oxide (FTO) substrates placed at an angle against the wall of a container with the conducting side facing down. The reaction was carried out at 180 ^oC by keeping the above autoclave in an electric oven for 2 hours. After the reaction the FTO/TNR substrate was taken out, washed 3 times with DI water, dried, and was annealed at 450 ^oC for 1 hr in the air. The obtained TNR films were used for further studies.

2.2. Plasma-functionalization of TNR surface:

To functionalize the TNR surface, an atmospheric pressure plasma jet was employed [67]. The radio frequency (RF) plasma jet with Helium carrier gas mixed with either oxygen or nitrogen was used in this process for surface modification. A RF field was applied between two stainless steel electrodes covered on the sides with quartz plates forming a gap of 1×1 mm^2 in cross section and 30 mm in length [77]. The plasma was ignited using a gas mixture of helium and oxygen, corresponding to flow rates of 3 slm and 30 sccm, respectively, with an input power of 10 watts. The distance between the jet and the substrate was maintained at 5 mm during the exposure for 5 mins.

2.3. Characterization:

The X-ray diffraction was carried out using Cu Kα radiation (BRUKER USA D8 Advance, Davinci, wavelength =1.5405 Å) with the diffraction angle from 10° to 80°. Absorption studies were carried out with the ultraviolet-diffuse reflectance spectroscopy (UV-DRS) by using Agilent-Cary (Cary 5000 UV-Vis-NIR) spectrophotometer. Raman spectra were recorded using Micro Raman spectrometer (HORIBA France, LABRAM HR Evolution) with a 532 nm laser

wavelength. The surface morphology of the film was studied by using a high-resolution Scanning Electron Microscope (F E I Quanta FEG 200). Water contact angle measuring instrument (HO-IAD-CAM-01) was used in this study to measure the wettability of TNR substrates before and after AP treatment. 1 mL of deionized water was dispensed for each measurement. The photoelectrochemical measurements of the TNR samples were recorded using CHI604E potentiostat with the scan rate of 50 mV/s and a scanning range of -1.0V to 1.5V. Photoelectrochemical cell had the platinum, Ag/AgCl, and TiO_2/FTO films used as a counter, reference, and working electrodes respectively. 0.1 M NaOH was used as the electrolyte throughout measurements and the light from a PET (Photo Emission Tech, Inc. USA, 300WSS-EM) solar simulator with power 100 mW/cm^2 was used for illumination under 1.5 AM filter.

3. Results and Discussion:

3.1 Structural and morphological study:

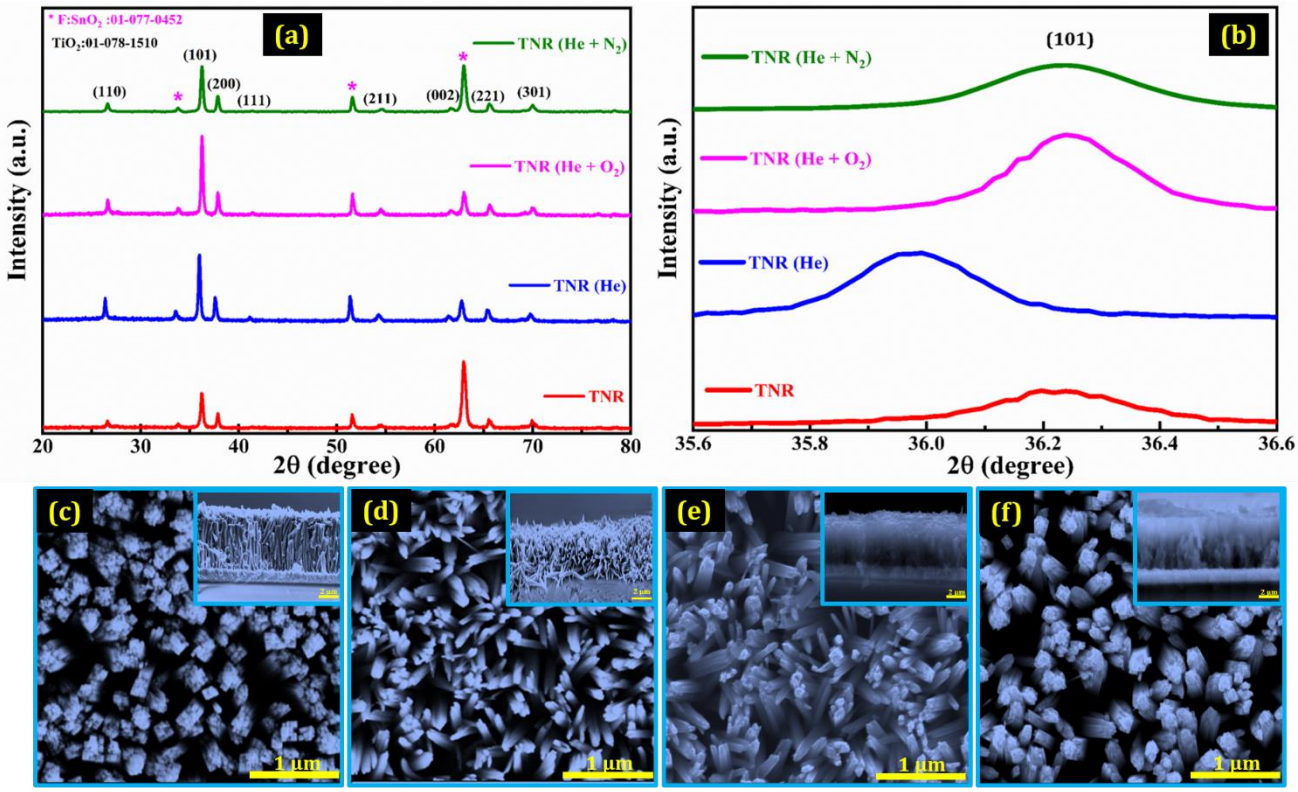

Fig.1. (a) XRD patterns with (b)overlay spectra of (101) plane & (c), (d), (e), (f) surface and (inset) cross-sectional FE-SEM images of the TNR, TNR(He), TNR(He + O_2) and TNR(He + N_2) films

Fig.1 (a) shows that the XRD patterns of TNR, TNR (He), TNR (He + O_2), and TNR (He + N_2) films were in accordance with the standard data for TiO_2 (space group; P42/mnm) as provided by JCPDS (Joint Committee on Powder Diffraction Standards), reference: 01-078-1510, thereby confirming tetragonal rutile phase of TiO_2. All the films exhibited crystalline nature having the most intense peak consistent to (101) plane of TiO_2. Six more peaks corresponding to (110), (200), (111), (211), (002), (221), (112) and (301) planes were also observed. No peaks were observed corresponding to anatase or brookite phase indicating the high purity of the rutile TNR samples. The crystallite size (D) was estimated by using Debye–Scherrer formula,

$$D = \frac{0.9\lambda}{\beta cos\Theta}$$

where, λ- 0.15418 nm, β- full width at half maximum (FWHM), and Θ- Bragg's angle in degree. Fig. 1(b) shows the overlay spectra of (101) plane and we estimated 2Θ values (36.26 °, 35.98 °, 36.25 ° & 36.23 °) FWHM (0.3085 °, 0.1278 °, 0.1299 ° & 0.2996 °) for (101) plane of TiO_2 (TNR, TNR (He), TNR (He + O_2), & TNR (He + N_2)). The observed shift in 2Θ values with respect to the untreated TNR was about 0.28 °, 0.01 ° & 0.03 ° after He, (He + O_2), & (He + N_2) APPJ treatments respectively. The shift in the 2Θ values can be attributed to the stress on the lattice caused due to the pressure exerted by the reactive gas used for the APPJ treatment. The calculated crystalline sizes for TNR, TNR (He), TNR (He + O_2), and TNR (He + N_2) films were 28.31, 68.29, 67.24, and 29.10 nm respectively. It can be noticed that the APPJ treatment caused observable changes in the crystalline size. He and He + O_2 plasma-treated samples showed bigger size crystals, more than double in size, as compared to the He + N_2 APPJ treated and untreated TNRs. This effect is similar to the observation with N_2 plasma-treated TiO_2 nanoparticles in the literature [78]. The increase in the crystalline size indicates the improvement in the crystallinity of TNRs and also can be related to the formation of intrinsic defects on the surface of TiO_2 itself referring to the similar observations in the literature [79]. The improved crystallinity with the formation of intrinsic defects after He and (He + O_2) APPJ treatment may lead to an improved PEC activity [80–82].

Fig. 1 (c, d, e & f) shows the surface and cross-sectional FE-SEM images of samples TNR, TNR (He), TNR (He + O_2), and TNR (He + N_2) films respectively. In the Fig. 1(c & f), we observed that the package of few TNR arrays which was vertically aligned perpendicular to the surface of the substrate. But, after He and (He + O_2) APPJ treatment the TNRs became slightly slanted &

separated from each other (Fig. 1(d &f)). For the calculation of diameter and length of TNRs, we have used imageJ software and an average value of 10 readings for each sample was taken. The APPJ treated and untreated TNR films showed the uniform distribution of vertical TiO_2 nanorods with a diameter of about 100 nm and the length of around 3 µm throughout the substrate [54]. As shown in Fig. 2, the TNRs were aligned perpendicular to the surface of the substrate and the alignment was changed slightly after the He atmospheric plasma treatment, where they became slightly slanted & separated from each other. The reason behind this change in morphology could be the longitudinal force exerted on the surface. This can be from the substantial gas velocity which caused by the high input gas pressure or adatoms by the ions in the plasma. Also, the etching which happens when the energetic ions hit the surface of TNRs could affect the morphology. Moreover, the transient electric field (EF) at the tip of plasma plume, typically in the kV/cm could not be neglected as well [83–85]. However, the observed change in morphology/alignment can offer an additional surface for the interaction of He APPJ treated TNRs with the electrolyte and form an effective TNR-electrolyte interface for the photoelectrochemical reaction. As we discussed in the introduction section, there is also a possibility that the changes in the alignment of nanorods might be detrimental for light absorption.

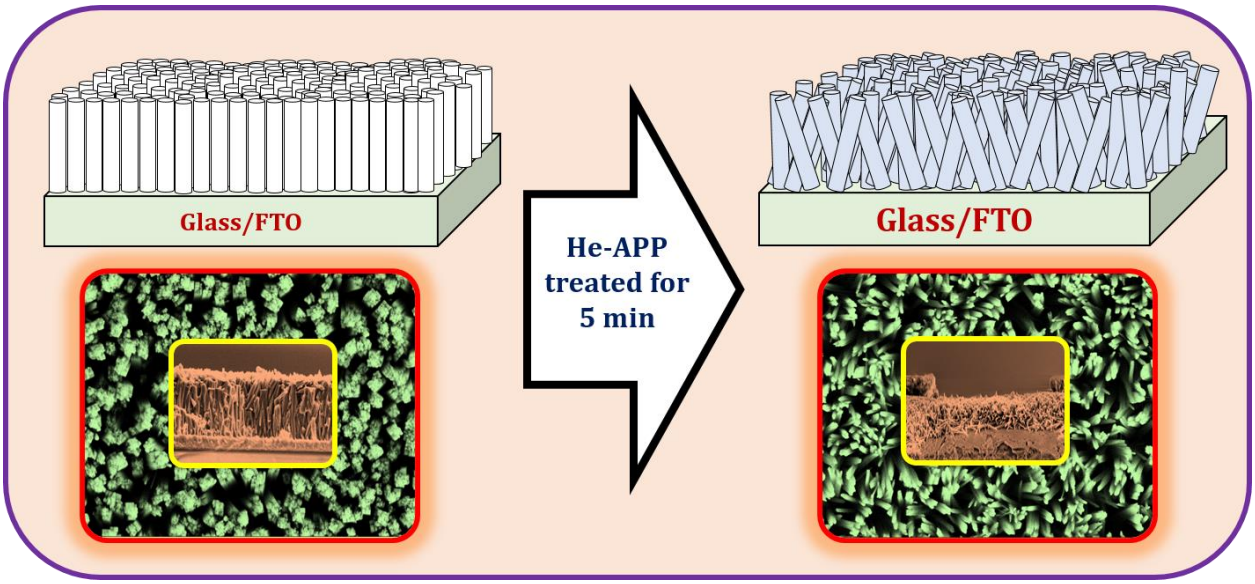

Fig.2. Schematic of the He-APP treatment of the TNR films

3.2 Optical study:

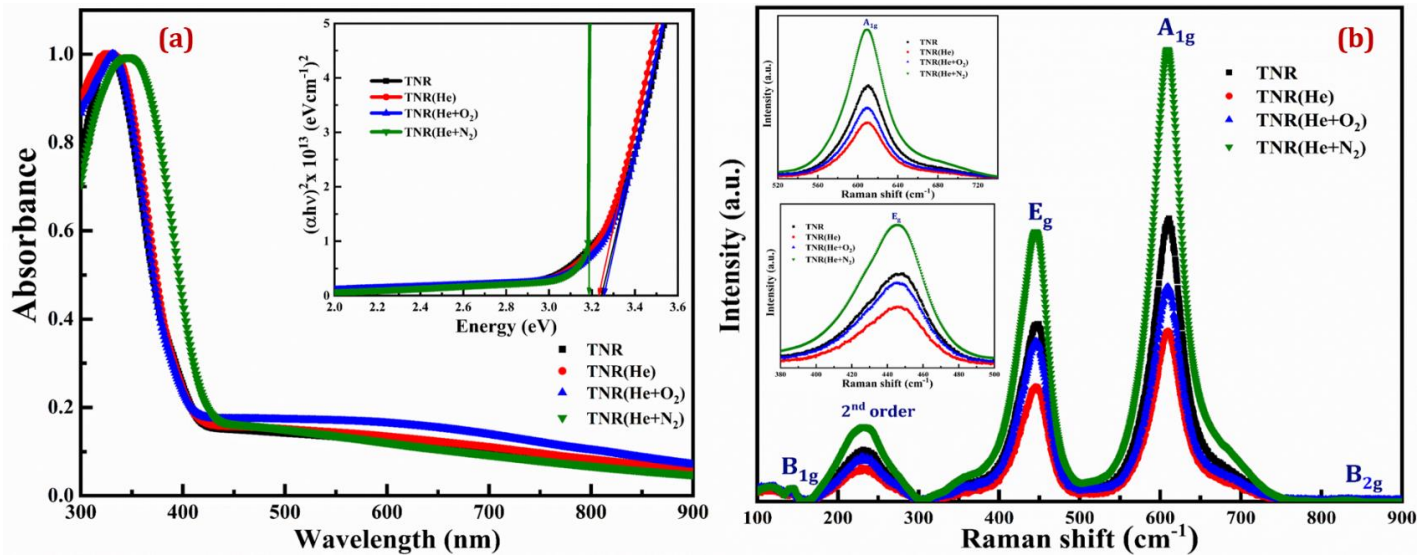

Fig.3. (a) UV-visible spectra with (inset) Tauc plot and (b) Raman spectra with an overlay of Raman spectra for A_{1g} & E_g modes of the TNR, TNR(He), TNR(He + O_2), and TNR(He + N_2) films.

The UV-visible absorbance spectra of treated and untreated TNR films over the wavelength range of from 300–900 nm is shown in Fig. 3(a). The bandgap of the TNR films has been determined using the relation,

$$\alpha = A\left(h\nu - E_g\right)^{\frac{1}{2}}$$

where, α is the absorption coefficient, A is the constant, E_g is the energy gap and $h\nu$ is the incident photon energy. The values of bandgap were estimated from the Tauc plots (inset of Fig. 3(a)) as 3.24, 3.22, 3.25, and 3.19 eV for the TNR, TNR (He), TNR (He + O_2), and TNR (He + N_2) films respectively, which are in accordance with the previous reports [86,87].

It can be observed that the absorption edge was shifted to higher wavelength (red shift) and the bandgap was reduced for TNR (He) as well as TNR (He+N_2) samples. In contrast, there was an increase in the bandgap (blue shift) for TNR (He+O_2). The possibility for such variation in the band edge after plasma treatment of TiO_2 is indicated in the literature and our results are in accordance with the same [20]. The plasma treatment was used as an effective technique to decrease the bandgap of TiO_2 and to promote the formation of defect states by introducing the oxygen vacancies

[62], both of which could improve the UV-visible light absorption [88,89]. Similar changes observed in our UV-visible absorption spectra of TNRs after the He and (He + N_2) APPJ treatment, where there was an improved absorption and red shift of band edge [65, 66] indicating the formation of oxygen vacancy defect states unlike in the case of (He + O_2) APPJ treatment. These changes observed in the UV-visible light absorption after the He and (He + N_2) APPJ treatment also indicate improved PEC activity, analogous to the earlier observation in the literature [62].

Fig.3 (b) shows the Raman spectra of the TNR, TNR (He), and TNR (He + O_2) films. Raman spectra of all the samples confirmed the formation of the rutile phase of TiO_2. There are five Raman active modes namely $A_{1g,}$ B_{1g}, B_{2g}, E_g, and multi-photon process mode for rutile TiO_2 [76,88,90], which appear around at 611 cm^{-1}, 143 cm^{-1}, 830 cm^{-1}, 447 $cm^{-1,}$ and 240 cm^{-1} respectively. The two prominent maxima at 447 cm^{-1} (E_g) and 611 cm^{-1} (A_{1g}) are in accordance with literature for rutile TiO_2 [76,91]. The A_{1g} peak position (Fig (b) inset) for TNR, TNR(He), TNR(He + O_2), and TNR(He + N_2) films appeared at 611.10, 609.16, 610.07, and 611.10 cm^{-1} with FWHM 27.42, 26.50, 28.75 and 38.86 cm^{-1}. Also, the E_g peak position (Fig (b) inset) appeared at 447.72, 445.23, 445.23 and 445.23 cm^{-1} with FWHM 32.30, 30.07, 32.95 and 23.24 cm^{-1} for TNR, TNR(He), TNR(He + O_2), and TNR(He + N_2) films respectively. The decrement in the FWHM of A_{1g} and E_g peaks indicated that the increment in the crystallinity of TNR after He APP, in concurrence with their XRD result as well as the literature report [76].

Surface wettability, as one of the fundamental surface properties of an electrode, could show significant influence on its functionalities such as electrolyte-wetting, redox electron transfer and gas release in electrochemical reactions [92–97]. Its known that a hydrophilic surface leads to better electron transfer rate between electrolyte and electrode [94]. The surface plasma treatment also improves the wettability of the TiO_2 photoanode by forming hydroxyl groups and could contribute to the enhancement of PEC performance [43]. Expecting the similar effect, we have performed the wettability test of untreated and APPJ treated TiO_2 NRs with water, and the results are shown in Fig. S1 (Supporting information). The contact angles of the water droplet for the APPJ treated TiO_2 NRs were smaller than that for the untreated TiO_2 NRs. He APPJ treatment showed a small change in wettability, and further optimization of plasma treatment conditions may be needed to achieve the hydrophilic nature of the TNR films. Lee et al. had observed a significant improvement in wettability of Ti substrate after plasma treatment by using He and O_2/He mixture carrier gases

[98]. Similarly, in our case wettability has improved after (He + O_2) & (He + N_2) APPJ treatment with a switch from hydrophobic to hydrophilic nature.

3.3 PEC measurements of TiO_2 films:

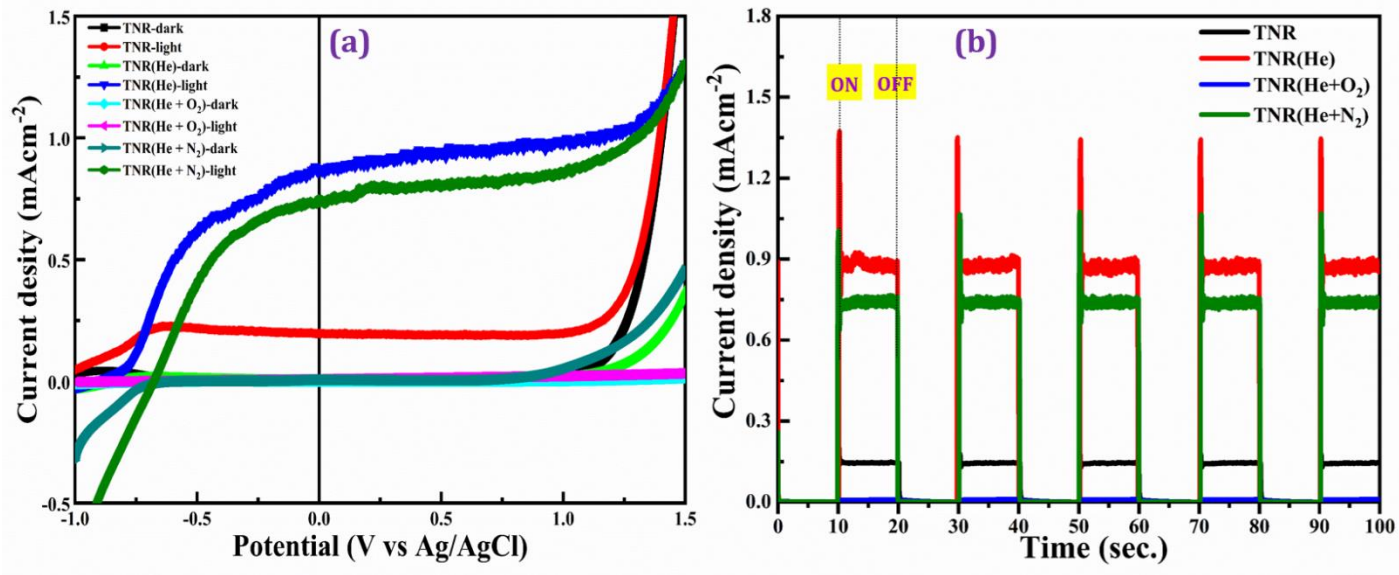

Fig.4. (a) Linear sweep voltammogram (LSV) curves and (b) Results from a chronoamperometry measurement of TNR, TNR(He), TNR(He + O_2), and TNR(He + N_2) films under light chopping for 10 seconds.

Fig. 4 (a) shows the linear sweep voltammogram (LSV) curves of the treated and untreated TNR samples in dark and under illumination. The maximum current density at 0 V (Ag/AgCl) observed for the TNR, TNR (He), TNR (He + O_2), and TNR (He + N_2) were 0.1964, 0.8715, 0.0079, and 0.7450 $mAcm^{-2}$ respectively. Further, chronoamperometry measurement was performed to check the stability and reproducibility of the photoanode. The measurement was carried out with 5 on-off cycles of 10 s time interval, in a similar manner as reported earlier on PEC devices [62,99]. Fig. 4(b) revealed the good reproducibility & stability of the current density with time. All treated and untreated TNR films were observed to be stable after 5 on-off cycles with a time duration of 10 seconds at 0.4 V (Ag/AgCl). We observed almost 4 times enhancement in the maximum current density for TNR (He) film as compared to untreated TNR under the light. At fixed potentials the electrodes usually adopt a steady dark current. In our case, we could observe that the current reached a sharp maximum (the current spike) immediately after switching on the light. This might

be attributed to the rapid initial separation of electron/hole pairs or to the presence of the high initial concentration of negative charge carriers accumulated in the film during the deposition [100]. Such spikes are known to arise due to the electron recombination with surface-trapped holes or photo-oxidation intermediates [101].

Based on our observations, this enhancement in the current density of the He-treated TNRs can be ascribed to the higher crystallinity, reduced bad gap, availability of additional surface area, and the possible formation of oxygen vacancy defect states in the TNRs. However, the TNR sample treated with (He + O_2) showed very less current density compared to all others, which may be due to the absence of oxygen vacancy defect states as indicated by the UV-visible absorption studies. Also, due to the lower crystallinity, as shown by the XRD & Raman results, TNR (He + N_2) samples exhibited lower current density compared to the TNR (He).

The results obtained are comparable with the previous reports in the literature (Table 1). It is noteworthy that the PEC activity of He plasma surface-modified TNRs was comparable to the best in the literature using ALD grown Hydrogen plasma-treated planar TiO_2. The photocurrent density shown by the He APPJ treated TNRs is the second-highest reported so far for TiO_2 and there is room for further improvement by optimization or employing the plasma of other carrier gases such as H_2, Ar, N_2, and O_2. The approach presented here for the first time by combining the simpler, greener, and a single step hydrothermal route for making the TNRs with the room temperature atmospheric pressure plasma functionalization technique can be explored for many other applications as well.

TiO_2	**Plasma modification**	**Max. photocurrent density ($mAcm^{-2}$)**	**Reference**
ALD grown planar TiO_2	As prepared	0.12 (0.8 V vs NHE)	[61]
	Hydrogen plasma for 1 hr at 200 ^oC	1.0 (0.8 V vs NHE)	
TiO_2 nanosheet	As prepared	0.113 (0.6 V vs Ag/AgCl)	[62]
	Argon plasma for 2 hr at 40 Pa	0.0437 (0.6 V vs Ag/AgCl)	
Mesoporous TiO_2	As prepared	0.00081(0.4 V vs Ag/AgCl)	[63]

	Hydrogen plasma for 5 min at 60mTorr	0.0229 (0.4 V vs Ag/AgCl)	
TiO_2 nanorods	As prepared	0.1964 (0 V vs Ag/AgCl)	**This work**
	Helium atmospheric pressure plasma for 5 min	0.8715 (0 V vs Ag/AgCl)	
	(Helium+ Oxygen) atmospheric pressure plasma for 5 min	0.0079 (0 V vs Ag/AgCl)	
	(Helium+ Nitrogen) atmospheric pressure plasma for 5 min	0.7450 (0 V vs Ag/AgCl)	

Table-1: Comparison of our photoelectrochemical results with literature

4. Conclusion:

In summary, surface functionalization of TNRs was achieved using the simple, room temperature atmospheric pressure plasma treatment technique. The effect of APP treatment on the structural, optical, and PEC properties of TNRs was established. A four-fold enhancement in the photocurrent was observed after the He-APPJ treatment of TNRs, and this performance is on par with the best in the literature using the conventional hydrogen plasma-treated ALD grown planar TiO_2. The improvement in the PEC performance could be correlated with our observations on (i) the availability of surplus surface area of TNRs to interact with the electrolyte, (ii) the increase in the crystalline size, accompanied by the possible formation of more intrinsic defects in TNRs and (iii) reduction in the bandgap which improved the UV-visible light absorption.

5. Acknowledgment:

SVB and VVS would like to acknowledge the research grant from the DST-SERB (File No. ECR/2015/000513), Government of India. SVB and SK acknowledge the support from the International Exchange grant of the Royal Society, UK (Ref.: IES\R2\170272). Authors also thank SRMIST for providing the necessary infrastructure and the characterization facilities such the micro-Raman spectrometer, the XRD facility set up with support from MNRE (Project No. 31/03/2014-15/PVSE-R&D) and the FE-SEM facility at the Nanotechnology Research Centre (NRC). Also, thanks to Dr. Sheela Singh, SRMIST for providing the contact angle measurement facility funded by DST-SERB (EMR/2016/001066). Authors also thank the INUP program and

the facilities such as FE-SEM at CeNSE, funded by Ministry of Electronics and Information Technology (MeitY), Govt. of India, and located at the Indian Institute of Science, Bengaluru. VG would like to acknowledge the DST-SERB (YSS/2015/000651) project, Government of India.

6. Data availability statement

The raw/processed data required to reproduce these findings cannot be shared at this time as the data also forms part of an ongoing study.

7. References:

[1] F. Shahvaranfard, M. Altomare, Y. Hou, S. Hejazi, W. Meng, B. Osuagwu, N. Li, C.J. Brabec, P. Schmuki, Engineering of the electron transport layer/perovskite interface in solar cells designed on TiO_2 rutile nanorods, Adv. Funct. Mater. 30 (2020) 1909738.

[2] C. Imparato, G. Iervolino, M. Fantauzzi, C. Koral, W. Macyk, M. Kobielusz, G. D'Errico, I. Rea, R. Di Girolamo, L. De Stefano, A. Andreone, V. Vaiano, A. Rossi, A. Aronne, Photocatalytic hydrogen evolution by co-catalyst-free TiO_2/C bulk heterostructures synthesized under mild conditions, RSC Adv. 10 (2020) 12519–12534.

[3] R. Nebel, K.M. Macounová, H. Tarábková, L. Kavan, P. Krtil, Selectivity of photoelectrochemical water splitting on TiO_2 anatase single crystals, J. Phys. Chem. C. 123 (2019) 10857–10867.

[4] J-B. Chemin, S. Bulou, K. Baba, C. Fontaine, T. Sindzingre, N.D. Boscher, P. Choquet, Transparent anti-fogging and self-cleaning TiO_2/SiO_2 thin films on polymer substrates using atmospheric plasma, Sci. Rep. 8 (2018) 9603.

[5] W.U. Huynh, J.U. Dittmer, A.P. Alivisatos, Hybrid nanorod-polymer solar cells, Science 295 (2002) 2425.

[6] Y. Lin, S. Zhou, X. Liu, S. Sheehan, D. Wang, TiO_2 /$TiSi_2$ heterostructures for high-efficiency photoelectrochemical H_2O splitting, J. Am. Chem. Soc. 131 (2009) 2772–2773.

[7] F. Sauvage, D. Chen, P. Comte, F. Huang, L-P. Heiniger, Y-B. Cheng, R.A. Caruso, M. Graetzel, Dye-sensitized solar cells employing a single silm of mesoporous TiO_2 beads achieve power conversion efficiencies over 10%, ACS Nano. 4 (2010) 4420–4425.

[8] Y. Zhang, W. Fu, H. Yang, Q. Qi, Y. Zeng, T. Zhang, R. Ge, G. Zou, Synthesis and

characterization of TiO_2 nanotubes for humidity sensing, Appl. Surf. Sci. 254 (2008) 5545–5547.

[9] K. Lee, J. Lim, H. Kim, T.L. Alford, G.E. Jabbour, K. Lee, J. Lim, H. Kim, T.L. Alford, G.E. Jabbour, Transparent conductive electrodes of mixed TiO_{2-x} – indium tin oxide for organic photovoltaics, Appl. Phys. Lett. 100 (2012) 213302.

[10] S. Rabaste, J. Bellessa, B. Brioude, C. Bovier, J.C. Plenet, R. Brenier, O. Marty, J. Mugnier, J. Dumas, Sol–gel fabrication of thick multilayers applied to Bragg reflectors and microcavities, Thin Solid Films. 416 (2002) 242–247.

[11] Y. Liao, X. Wang, Y. Ma, J. Li, T. Wen, L. Jia, Z. Zhong, L. Wang, D. Zhang, New mechanistic insight of low temperature crystallization of anodic TiO_2 nanotube array in water, Cryst. Growth Des. 16 (2016) 1786–1791.

[12] A. Gültekin, S. Sönmezoğlu, Titanium dioxide thin films containing gold-silver nanoclusters by sol–gel technique, Z. Phys. Chem. 228 (2014) 649–662.

[13] B. Liu, E.S. Aydil, Growth of oriented single-crystalline rutile TiO_2 nanorods on transparent conducting substrates for dye-sensitized solar cells, J. Am. Chem. Soc. 131 (2009) 3985–3990.

[14] H.-S. Kim, J.-W. Lee, N. Yantara, P.P. Boix, S.A. Kulkarni, S. Mhaisalkar, M. Grätzel, N.-G. Park, High efficiency solid-state sensitized solar cell-based on submicrometer rutile TiO_2 nanorod and $CH_3NH_3PbI_3$ Perovskite sensitizer, Nano Lett. 13 (2013) 2412–2417.

[15] S.S. Mali, C.S. Shim, H.K. Park, J. Heo, C.K. Hong, Ultrathin atomic layer deposited TiO_2 for surface passivation of hydrothermally grown 1D TiO_2 nanorod arrays for efficient solid state perovskite solar cells, Chem. Mater. 27 (2015) 1541–1551.

[16] Y. Tak, J. Hong, S. Lee, K. Yong, Fabrication of ZnO/CdS core/shell nanowire arrays for efficient solar energy conversion, J. Mater. Chem. 19 (2009) 5945–5951.

[17] T.-L. Li, Y.-L. Lee, H. Teng, $CuInS_2$ quantum dots coated with CdS as high-performance sensitizers for TiO_2 electrodes in photoelectrochemical cells, J. Mater. Chem. 21 (2011) 5089–5098.

[18] J-B. Han, X. Wang, N. Wang, Z-H. Wei, G.-P. Yu, Z-G. Zhou, Q-Q. Wang, Effect of plasma treatment on hydrophilic properties of TiO_2 thin films, Surf. Coat. Tech. 200 (2006) 4876–4878.

[19] B. Wang, S. Shen, S.S. Mao, Black TiO_2 for solar hydrogen conversion, J Mater. 3 (2017)

96–111.

[20] B. Bharti, S. Kumar, H-N. Lee, R. Kumar, Formation of oxygen vacancies and Ti^{3+} state in TiO_2 thin film and enhanced optical properties by air plasma treatment, Sci. Rep. 6 (2016) 32355.

[21] Y. Liu, J. Wang, P. Yang, K. Matras-Postolek, Self-modification of TiO_2 one-dimensional nano-materials by Ti^{3+} and oxygen vacancy using Ti_2O_3 as precursor, RSC Adv. 5 (2015) 61657–61663.

[22] X. Lu, G. Wang, T. Zhai, M. Yu, J. Gan, Y. Tong, Y. Li, Hydrogenated TiO_2 nanotube arrays for supercapacitors, Nano Lett. 12 (2012) 1690–1696.

[23] M. Konstantakou, T. Stergiopoulos, V. Likodimos, G.C. Vougioukalakis, L. Sygellou, A.G. Kontos, A. Tserepi, P. Falaras, Influence of fluorine plasma treatment of TiO_2 films on the behavior of dye solar cells employing the Co(II)/(III) redox couple, J. Phys. Chem. C. 118 (2014) 16760–16775.

[24] G.S. Selwyn, H.W. Herrmann, J. Park, I. Henins, Materials processing using an atmospheric pressure, RF-generated plasma source, Contrib. to Plasma Phys. 41 (2001) 610–619.

[25] L.M. Zhou, B. Xue, U. Kogelschatz, B. Eliasson, Nonequilibrium plasma reforming of greenhouse gases to synthesis gas, Energy and Fuels. 12 (1998) 1191–1199.

[26] G.B. Zhao, S. John, J.J. Zhang, L. Wang, S. Muknahallipatna, J.C. Hamann, J.F. Ackerman, M.D. Argyle, O.A. Plumb, Methane conversion in pulsed corona discharge reactors, Chem. Eng. J. 125 (2006) 67–79.

[27] Y.P. Zhang, Y. Li, Y. Wang, C.J. Liu, B. Eliasson, Plasma methane conversion in the presence of carbon dioxide using dielectric-barrier discharges, Fuel Process. Technol. 83 (2003) 101–109.

[28] C. Qi, D. Wei, T. Xumei, H. Yu, D. Xiaoyan, Y. Yongxiang, CO_2 Reforming of CH_4 by atmospheric Abnormal Glow Plasma, Plasma Sci. Technol. 181 (2006).

[29] D. Li, X. Li, M. Bai, X. Tao, S. Shang, X. Dai, Y. Yin, CO_2 reforming of CH_4 by atmospheric pressure glow discharge plasma: A high conversion ability, Int. J. Hydrogen Energy. 34 (2009) 308–313.

[30] M.W. Li, G.H. Xu, Y.L. Tian, L. Chen, H.F. Fu, Carbon Dioxide Reforming of Methane Using DC Corona Discharge Plasma Reaction, J. Phys. Chem. A. 108 (2004) 1687–1693.

[31] Y. Li, C.J. Liu, B. Eliasson, Y. Wang, Synthesis of oxygenates and higher hydrocarbons

directly from methane and carbon dioxide using dielectric-barrier discharges: Product distribution, Energy and Fuels. 16 (2002) 864–870.

[32] Y. Li, G. Xu, C. Liu, B. Eliasson, B. Xue, Co-generation of syngas and higher hydrocarbons from CO_2 and CH_4 using dielectric-barrier discharge: Effect of electrode materials, Energy and Fuels. 15 (2001) 299–302.

[33] H. Le, L.L. Lobban, R.G. Mallinson, Some temperature effects on stability and carbon formation in low temperature ac plasma conversion of methane, Catal. Today. 89 (2004) 15–20.

[34] A. Huang, G. Xia, J. Wang, S.L. Suib, Y. Hayashi, H. Matsumoto, CO_2 reforming of CH_4 by atmospheric pressure ac discharge plasmas, J. Catal. 189 (2000) 349–359.

[35] J.R. Fincke, R.P. Anderson, T. Hyde, B.A. Detering, R. Wright, R.L. Bewley, D.C. Haggard, W.D. Swank, Plasma Thermal Conversion of Methane to Acetylene, Plasma Chem. Plasma Process. 22 (2002) 105–136.

[36] D. Bin, Z. Xiu-ling, G. Wei-min, H. Ren, Study on the Methane Coupling under Pulse Corona Plasma by Using CO_2 as Oxidant, Plasma Sci. Technol. 2 (2000) 577–580.

[37] C.A. Beaudette, X. Wang, U.R. Kortshagen, Nanocrystal-based inorganic nanocomposites: A new paradigm for plasma-produced optoelectronic thin films, Plasma Process. Polym. 17 (2020) 1–9.

[38] S. Bekeschus, P. Favia, E. Robert, T. von Woedtke, White paper on plasma for medicine and hygiene: Future in plasma health sciences, Plasma Process. Polym. 16 (2019) 1–12.

[39] H.-U. Kim, C. Yi, S.-W. Rhee, The effect of He or Ar/O_2 plasma treatment on Si surface prior to chemical vapor deposition of SiO_2, J. Mater. Sci. Mater. Electron. 15 (2004) 37–41.

[40] C.M. Chan, T.M. Ko, H. Hiraoka, Polymer surface modification by plasmas and photons, Surf. Sci. Rep. 24 (1996) 1–54.

[41] C. Oehr, Plasma surface modification of polymers for biomedical use, Nucl. Instrum. Methods Phys. Res., B. 208 (2003) 40–47.

[42] I. Pashkuleva, A.P. Marques, V. Filipe, R.L. Reis, Surface modification of starch based biomaterials by oxygen plasma or UV-irradiation, J Mater Sci Mater Med. 21 (2010) 21–32.

[43] T. Zhang, S. Cui, B. Yu, Z. Liu, D. Wang, Surface engineering for enhanced photoelectrochemical response of TiO_2 nanotube arrays by simple surface air plasma

treatment, Chem. Commun. 51 (2015) 16940–16943.

[44] Y. Kim, B. Jin, R. Vittal, Y. Lee, N. Park, K. Kim, Low-temperature oxygen plasma treatment of TiO_2 film for enhanced performance of dye-sensitized solar cells, J. Power Sources. 175 (2008) 914–919.

[45] K. Ahn, H.-U. Lee, S-Y. Jeong, J-P. Kim, J.S. Jin, H-S. Ahn, H-S. Kim, C-R. Cho, Plasma treatment effect on dye-sensitized solar cell efficiency of hydrothermal-processed TiO_2 nanorods, J. Nanosci. Nanotechnol. 12 (2012) 6022–6025.

[46] L. Zhao, W. Dong, F. Zheng, L. Fang, M. Shen, Interrupted growth and photoelectrochemistry of Cu_2O and Cu particles on TiO_2, Electrochim. Acta. 80 (2012) 354–361.

[47] D. Jiang, S. Zhang, Z. Huijun, Photocatalytic degradation characteristics of different organic compounds at TiO_2 nanoporous film electrodes with mixed anatase/rutile phases, Environ. Sci. Technol. 41 (2007) 303–308.

[48] D.-N. Bui, S.-Z. Kang, X. Li, J. Mu, Effect of Si doping on the photocatalytic activity and photoelectrochemical property of TiO_2 nanoparticles, Catal. Commun. 13 (2011) 14–17.

[49] F. Gracia, J.P. Holgado, A. Caballero, A.R. Gonzalez-Elipe, Structural, optical, and photoelectrochemical properties of M^{n+}-TiO_2 model thin film photocatalysts, J. Phys. Chem. B. 108 (2004) 17466–17476.

[50] Y. Wang, H. Cheng, Y. Hao, J. Ma, W. Li, S. Cai, Preparation , characterization and photoelectrochemical behaviors of Fe (III)-doped TiO_2 nanoparticles, J. Mater. Sci. 34 (1999) 3721–3729.

[51] J.Y. Bae, T.K. Yun, K.S. Ahn, J.H. Kim, Visible-photoresponsive nitrogen-doped mesoporous TiO_2 films for photoelectrochemical cells, Bull. Korean Chem. Soc. 31 (2010) 925–928.

[52] A.V. Vinogradov, V.V. Vinogradov, A.V. Agafonov, A simple preparation of highly photoactive Fe (III)-doped titania nanocrystals by annealing-free approach, J. Alloy. 581 (2013) 675–678.

[53] Y-P. Peng, Y-T. Yeh, I.S. Shah, C.P. Huang, Concurrent photoelectrochemical reduction of CO_2 and oxidation of methyl orange using nitrogen-doped TiO_2, Appl. Catal. 123–124 (2012) 414–423.

[54] S. Hoang, S.P. Berglund, N.T. Hahn, A.J. Bard, C.B. Mullins, Enhancing visible light

photo-oxidation of water with TiO_2 nanowire arrays via cotreatment with H_2 and NH_3: Synergistic effects between Ti^{3+} and N, J. Am. Chem. Soc. 134 (2012) 3659–3662.

[55] C. Cheng, Y. Sun, Carbon doped TiO_2 nanowire arrays with improved photoelectrochemical water splitting performance, Appl. Surf. Sci. 263 (2012) 273–276.

[56] M. Xu, H. Wu, D. Zhao, G. Zheng, Controlled Sn-doping in TiO_2 nanowire photoanodes with enhanced photoelectrochemical conversion, Nano Lett. 12 (2012) 1503–1508.

[57] C. Chen, Y. Wei, G. Yuan, Q. Liu, R. Lu, X. Huang, Y. Cao, P. Zhu, Synergistic effect of Si doping and heat treatments enhances the photoelectrochemical water oxidation performance of TiO_2 nanorod arrays, Adv. Funct. Mater. 27 (2017) 1701575.

[58] Y. Wang, Y. Zhang, J. Tang, H. Wu, M. Xu, Z. Peng, X. Gong, G. Zheng, Simultaneous etching and doping of TiO_2 nanowire arrays for enhanced photoelectrochemical performance, ACS Nano. 7 (2013) 9375–9383.

[59] I.S. Cho, C.H. Lee, Y. Feng, M. Logar, P.M. Rao, L. Cai, D.R. Kim, R. Sinclai, X. Zheng, Codoping titanium dioxide nanowires with tungsten and carbon for enhanced photoelectrochemical performance, Nat. Commun. 4 (2013) 1723.

[60] X. Wang, S. Estradé, Y. Lin, F. Yu, L. Lopez-conesa, H. Zhou, S.K. Gurram, F. Peiró, Z. Fan, H. Shen, L. Schaefer, G. Braeuer, A. Waag, Enhanced photoelectrochemical behavior of H-TiO_2 nanorods hydrogenated by controlled and local rapid thermal annealing, Nanoscale Res. Lett. 12 (2017) 336.

[61] A. Sasinska, T. Singh, S. Wang, S. Mathur, R. Kraehnert, Enhanced photocatalytic performance in atomic layer deposition grown TiO_2 thin films via hydrogen plasma treatment, J.Vac.Sci.Technol.A. 33 (2015) 01A152.

[62] X. Kong, Y. Xu, Z. Cui, Z. Li, Y. Liang, Z. Gao, S. Zhu, X. Yang, Defect enhances photocatalytic activity of ultrathin TiO_2 (B) nanosheets for hydrogen production by plasma engraving method, Appl. Catal. 230 (2018) 11–17.

[63] S.Z. Islam, A.R.S. Nagpure, N. Wanninayake, J.F. Browning, J. Strzalka, D.Y. Kim, S.E. Rankin, Hydrogen incorporation by plasma treatment gives mesoporous black TiO_2 thin films with visible photoelectrochemical water oxidation activity, Micropor. Mesopor. Mat. 261 (2018) 35–43.

[64] H. Jeong, B. Lee, Y. Lee, J. Lee, M. Yang, I. Kang, M. Mativenga, J. Jang, Coplanar amorphous-indium-gallium-zinc-oxide thin film transistor with He plasma treated heavily

doped layer coplanar amorphous-indium-gallium-zinc-oxide thin film transistor with He plasma treated heavily doped layer, Appl. Phys. Lett. 104 (2014) 022115.

[65] S. Shinya, T. Kaneko, M. Koyama, T. Maemoto, S. Sasa, Effects of He plasma treatment on zinc oxide thin film transistors, 2017 IEEE Int. Meet. Futur. Electron Devices, Kansai. 29 (2017) 66–67.

[66] S. Kajita, Y. Tomita, E. Yasunaga, T. Yoshida, K. Miyaguchi, H. Tanaka, N. Ohno, Photocatalytic decomposition of ethylene using He plasma induced nano-TiO_2, Jpn J Appl Phys. 58 (2019) 070903.

[67] A. Dey, P. Ghosh, J. Bowen, N.S.J. Braithwaite, S. Krishnamurthy, Engineering work function of graphene oxide from p to n type using a low power atmospheric pressure plasma jet, Phys.Chem.Chem.Phys. 22 (2020) 7685.

[68] P. Ghosh, A. Ivaturi, D. Bhattacharya, J. Bowen, T. Nixon, J. Kowal, N.S.J. Braithwaite, S. Krishnamurthy, Efficient hole transport material formed by atmospheric pressure plasma functionalization of Spiro-OMeTAD, Mater. Today Chem. 17 (2020) 100321.

[69] A. Dey, A. Chroneos, N.S.J. Braithwaite, R.P. Gandhiraman, S. Krishnamurthy, Plasma engineering of graphene, Appl. Phys. Rev. 3 (2016) 021301.

[70] A. Dey, G. Chandrabose, L. A.O Damptey, E.S. Erakulan, R. Thapa, S. Zhuk, G. Kumar Dalapati, S. Ramakrishna, N. St. J. Braithwaite, A. Shirzadi, S. Krishnamurthy, Cu_2O/CuO heterojunction catalysts through atmospheric pressure plasma induced defect passivation, Appl. Surf. Sci. (2020) 148571.

[71] J. Laimer, H. Sto, Recent advances in the research on non-equilibrium atmospheric pressure plasma jets, Plasma Process. Polym. 4 (2007) 266–274.

[72] M. Ghasemi, P. Olszewski, J.W. Bradley, J.L. Walsh, Interaction of multiple plasma plumes in an atmospheric pressure plasma jet array, J. Phys. D. Appl. Phys. 46 (2013).

[73] Z. Cao, Q. Nie, D.L. Bayliss, J.L. Walsh, C.S. Ren, D.Z. Wang, M.G. Kong, Spatially extended atmospheric plasma arrays, Plasma Sources Sci. Technol. 19 (2010).

[74] E. Robert, T. Darny, S. Dozias, S. Iseni, J.M. Pouvesle, New insights on the propagation of pulsed atmospheric plasma streams: From single jet to multi jet arrays, Phys. Plasmas. 22 (2015).

[75] A.V. Omran, G. Busco, L. Ridou, S. Dozias, C. Grillon, J.M. Pouvesle, E. Robert, Cold atmospheric single plasma jet for RONS delivery on large biological surfaces, Plasma

Sources Sci. Technol. 29 (2020).
[76] T.S. Bhat, R.S. Devan, S.S. Mali, A.S. Kamble, S.A. Pawar, I.Y. Kim, Y.R. Ma, C.K. Hong, J.H. Kim, P.S. Patil, Photoelectrochemically active surfactant free single step hydrothermal mediated titanium dioxide nanorods, J. Mater. Sci. Mater. Electron. 25 (2014) 4501–4511.
[77] D. Marinov, N.S.J. Braithwaite, Power coupling and electrical characterization of a radio-frequency micro atmospheric pressure plasma jet, Plasma Sources Sci. Technol. 23 (2014).
[78] R. Trejo-Tzab, L. Caballero-Espada, P. Quintana, A. Ávila-Ortega, R.A. Medina-Esquivel, Controlled phase changes of Titania using nitrogen plasma, Nanoscale Res. Lett. 12 (2017) 32.
[79] A. Testino, I.R. Bellobono, V. Buscaglia, C. Canevali, M.D. Arienzo, S. Polizzi, F. Scotti, Roberto and Morazzon, Optimizing the photocatalytic properties of hydrothermal TiO_2 by the control of phase composition and particle morphology . A systematic approach, J. Am. Chem. Soc. 129 (2007) 3564–3575.
[80] M. Maria Angelin Sinthiya, N. Kumaresan, K. Ramamurthi, K. Sethuraman, S. Moorthy Babu, R. Ramesh Babu, V. Ganesh, Influence of heat treatment on the properties of hydrothermally grown 3D/1D TiO_2 hierarchical hybrid microarchitectures over TiO_2 seeded FTO substrates, Appl. Surf. Sci. 449 (2018) 122–131.
[81] X. Sun, Q. Sun, Q. Zhang, Q. Zhu, H. Dong, L. Dong, Significant effects of reaction temperature on morphology , crystallinity , and photoelectrical properties of rutile TiO_2 nanorod array films, J. Phys. D Appl. Phys. 46 (2013) 095102.
[82] Y. Wang, L. Zhang, K. Deng, X. Chen, Z. Zou, Low temperature synthesis and photocatalytic activity of rutile TiO_2 nanorod superstructutes, J. Phys. Chem. C. 111 (2007) 2709–2714.
[83] A. Bourdon, T. Darny, F. Pechereau, J.M. Pouvesle, P. Viegas, S. Iséni, E. Robert, Numerical and experimental study of the dynamics of a μs helium plasma gun discharge with various amounts of N_2 admixture, Plasma Sources Sci. Technol. 25 (2016).
[84] B.M. Obradović, S.S. Ivković, M.M. Kuraica, Spectroscopic measurement of electric field in dielectric barrier discharge in helium, Appl. Phys. Lett. 92 (2008) 2–5.
[85] T. Darny, J.M. Pouvesle, V. Puech, C. Douat, S. Dozias, E. Robert, Analysis of conductive target influence in plasma jet experiments through helium metastable and electric field measurements, Plasma Sources Sci. Technol. 26 (2017).

[86] J-J. Wu, C.-C. Yu, Aligned TiO_2 nanorods and nanowalls, J. Phys. Chem. B. 108 (2004) 108–110.

[87] B. Chen, W. Niu, Z. Lou, Z. Ye, L. Zhu, Improving the photovoltaic performance of the all solid-state TiO_2 NRs/$CuInS_2$ solar cell by hydrogen plasma treatment, Nanotechnology. 29 (2018).

[88] X. Chen, L. Liu, P.Y. Yu, S.S. Mao, Increasing solar absorption for photocatalysis with black hydrogenated Titanium dioxide nanocrystals, Science 331 (2011) 746–750.

[89] A. Naldoni, M. Allieta, S. Santangelo, M. Marelli, F. Fabbri, S. Cappelli, C.L. Bianchi, R. Psaro, V.D. Santo, Effect of nature and location of defects on bandgap narrowing in black TiO_2 nanoparticles, J. Am. Chem. Soc. 134 (2012) 7600−7603.

[90] S.S. Mali, C.A. Betty, P.N. Bhosalec, P.S. Patil, Hydrothermal synthesis of rutile TiO2 with hierarchical microspheres and their characterization, CrystEngComm. 13 (2011) 6349–6351.

[91] H.L. Ma, J.Y. Yang, Y. Dai, Y.B. Zhang, B. Lu, G.H. Ma, Raman study of phase transformation of TiO_2 rutile single crystal irradiated by infrared femtosecond laser, Appl. Surf. Sci. 253 (2007) 7497–7500.

[92] Y. Wu, K. Liu, B. Su, L. Jiang, Superhydrophobicity-mediated electrochemical reaction along the solid-liquid-gas triphase interface: Edge-growth of gold architectures, Adv. Mater. 26 (2014) 1124–1128.

[93] K.A. Stoerzinger, W.T. Hong, G. Azimi, L. Giordano, Y.L. Lee, E.J. Crumlin, M.D. Biegalski, H. Bluhm, K.K. Varanasi, Y. Shao-Horn, Reactivity of Perovskites with Water: Role of Hydroxylation in Wetting and Implications for Oxygen Electrocatalysis, J. Phys. Chem. C. 119 (2015) 18504–18512.

[94] G. Sakuma, Y. Fukunaka, H. Matsushima, Nucleation and growth of electrolytic gas bubbles under microgravity, Int. J. Hydrogen Energy. 39 (2014) 7638–7645.

[95] C. Meng, B. Wang, Z. Gao, Z. Liu, Q. Zhang, J. Zhai, Insight into the Role of Surface Wettability in Electrocatalytic Hydrogen Evolution Reactions Using Light-Sensitive Nanotubular TiO_2 Supported Pt Electrodes, Sci. Rep. 7 (2017) 1–8.

[96] X. Feng, J. Zhai, L. Jiang, The fabrication and switchable superhydrophobicity of TiO_2 nanorod films, Angew. Chemie - Int. Ed. 44 (2005) 5115–5118.

[97] C.M. Ding, M.L. Lv, Y. Zhu, L. Jiang, H. Liu, Wettability-regulated extracellular electron

transfer from the living organism of shewanella loihica PV-4, Angew. Chemie - Int. Ed. 54 (2015) 1446–1451.

[98] H-Y. Lee, J-W. Ok, H-J. Lee, G.C. Kim, H.J. Lee, Surface treatment of a Titanium implant using a low temperature atmospheric pressure plasma jet, Appl. Sci. Converg. Technol. 25 (2016) 51–55.

[99] W. Xia, H. Qian, X. Zeng, J. Dong, J. Wang, Q. Xu, Visible-Light Self-Powered Photodetector and Recoverable Photocatalyst Fabricated from Vertically Aligned Sn_3O_4 Nanoflakes on Carbon Paper, J. Phys. Chem. C. 121 (2017) 19036–19043.

[100] S. Kment, P. Kluson, Z. Hubicka, J. Krysa, M. Cada, I. Gregora, A. Deyneka, Z. Remes, H. Zabova, L. Jastrabik, Double hollow cathode plasma jet-low temperature method for the $TiO_{2-x}N_x$ photoresponding films, Electrochim. Acta. 55 (2010) 1548–1556.

[101] T. Berger, D. Monllor-Satoca, M. Jankulovska, T. Lana-Villarreal, R. Gómez, The electrochemistry of nanostructured titanium dioxide electrodes, ChemPhysChem. 13 (2012) 2824–2875.